The Molecular Mechanism of Monolayer-Bilayer Transformations of Lung Surfactant from Molecular Dynamics Simulations

Svetlana Baoukina,* Luca Monticelli,* Matthias Amrein,† and D. Peter Tieleman*
*Department of Biological Sciences, University of Calgary, Calgary, Alberta, Canada, T2N 1N4; and †Department of Cell Biology and Anatomy, Faculty of Medicine, University of Calgary, Calgary, Alberta, Canada, T2N 1N4

ABSTRACT The aqueous lining of the lung surface exposed to the air is covered by lung surfactant, a film consisting of lipid and protein components. The main function of lung surfactant is to reduce the surface tension of the air-water interface to the low values necessary for breathing. This function requires the exchange of material between the lipid monolayer at the interface and lipid reservoirs under dynamic compression and expansion of the interface during the breathing cycle. We simulated the reversible exchange of material between the monolayer and lipid reservoirs under compression and expansion of the interface. We used a mixture of dipalmitoyl-phosphatidylcholine, palmitoyl-oleoyl-phosphatidylglycerol, cholesterol, and surfactant-associated protein C as a functional analog of mammalian lung surfactant. In our simulations, the monolayer collapses into the water subphase on compression and forms bilayer folds. On monolayer reexpansion, the material is transferred from the folds back to the interface. The simulations indicate that the connectivity of the bilayer aggregates to the monolayer is necessary for the reversibility of the monolayer-bilayer transformation. The simulations also show that bilayer aggregates are unstable in the air subphase and stable in the water subphase.

INTRODUCTION

Gas exchange takes place at the internal surface of the alveoli, small globular structures that terminate airways in the lungs. The alveolar epithelial cells are covered by a thin hydration layer exposed to the air. In the absence of surfactant, this air-water interface is unstable because of the high surface tension (~72 mN/m) and the small radius of the alveolus (~100 μm). Thus, the surface tension needs to be reduced to prevent the collapse of the alveoli as a result of the Laplace pressure.

Lung surfactant is a complex mixture of lipids and peptides forming a monolayer at the air-water interface of the alveoli (1). Its main physiological function is the reduction of the surface tension at the air-water interface of the lung. During the breathing cycle, lung surfactant maintains a low surface tension (0–10 mN/m) under dynamic compression and expansion of the interface (2). This function is believed to be associated with the exchange of material with lipid reservoirs that are attached to the monolayer (3–6).

The ''squeeze-out'' model of lung surfactant suggests that the monolayer undergoes a compositional change on compression: the unsaturated lipids are squeezed out from the interface, and the monolayer becomes highly enriched in dipalmitoyl-phosphatidylcholine (DPPC) (7–9). At physiological temperatures DPPC can pack tightly at the interface to form a liquid-condensed phase with a near-zero tension in a monolayer. However, recent experimental findings contradict the ''squeeze-out'' model (10–12) by showing that, at low surface tension, surfactant monolayer has several components and has both liquid-expanded and liquid-condensed phases. Lipid reservoirs connected to the monolayer have also been associated with the stability of the highly compressed monolayer (4,6,13). Atomic force microscopy (AFM) experiments have shown that these reservoirs are discontinuous lipid lamellar stacks containing one or several bilayers (6,13). They are distributed over the surface of the monolayer and formed on monolayer compression.

These monolayer-associated bilayer reservoirs are absent in surfactant with impaired function (4), characteristic of adult respiratory distress syndrome (14,15). Hence, understanding the molecular mechanism of the monolayer-bilayer transformation and the structure of the monolayer-bilayer aggregates may be important for treatment of patients with acute respiratory failure.

Detailed information on the monolayer-bilayer transformation in lung surfactant is not available directly from experiments. First, it is not clear whether the lipid reservoirs are formed in the air subphase or in the water subphase. Second, the structure of highly curved lipid regions connecting lipid reservoirs to the monolayer is difficult to study using current experimental techniques. Third, the role of different lipid and protein constituents in the formation of lipid reservoirs and their connectivity to the monolayer are not fully understood.

Here, we investigate the structure of a lung surfactant model and the mechanism of monolayer-bilayer transformation using molecular dynamics simulations. Previous simulations of lung surfactant focused on specific interactions of the surfactant-associated peptides with lipid monolayers (16–18). These simulations used atomistic models and investigated relatively small systems (box lateral size smaller than 10 nm) on time

Submitted May 22, 2007, and accepted for publication July 17, 2007.

Address reprint requests to D. Peter Tieleman, Department of Biological Sciences, University of Calgary, 2500 University Drive NW, Calgary, Alberta, Canada, T2N 1N4. E-mail: tieleman@ucalgary.ca.

Editor: Helmut Grubmuller.

0006-3495/07/12/3775/08 $2.00

doi: 10.1529/biophysj.107.113399

scales up to 30 ns. Mesoscopic time and length scales are required to study the monolayer-bilayer transition and the stability of the monolayer-associated bilayer aggregates. To reach these time and length scales, we use a coarse-grained (CG) molecular model that accurately reproduces the structure and dynamics of various lipid assemblies and lipid phase transitions (19–21). The model also reproduces the pressure-area isotherm for a DPPC monolayer (36). We simulated a model system consisting of DPPC, palmitoyl-oleoyl-phosphatidylglycerol (POPG), cholesterol (8:2:1 DPPC:POPG: cholesterol), and surfactant-associated protein C (SP-C). Despite the simple composition, this system is a functional analog to bovine lipid extract surfactant (BLES) (22). We simulate the formation of monolayer-associated bilayer reservoirs in the water subphase under monolayer compression. We show that lipid aggregates are unstable in the air subphase and thus are likely to be formed only in the water subphase.

METHODS

General system setup

The model system for lung surfactant consisted of CG DPPC and POPG lipids and cholesterol in the proportion 8:2:1, and CG SP-C proteins with palmitoylated chains. The simulation setup included a water slab bounded by two vacuum slabs with two symmetric monolayers at the two water-vacuum interfaces (Fig. 1). To study the mechanism of monolayer-bilayer transformation, the system was compressed or expanded to change the area available for the monolayers at the two interfaces without changing the box size in the normal direction. To investigate the properties and the evolution of the structure of the compressed/expanded monolayers, the monolayers were simulated at the constant volume of the simulation box with constant areas of the two interfaces and a fixed box size in the direction normal to the interfaces. To study the stability of lipid reservoirs associated with lung surfactant in the water and in the air subphases, we added preformed lipid aggregates to the system with two surfactant monolayers. In the first case, a circular bilayer patch was placed in the water subphase adjacent to one of the monolayers. In the second case, an inverted circular bilayer patch was placed in the vacuum subphase adjacent to one of the monolayers. In both cases, the lipid reservoirs had the same composition as the monolayers. These two systems were simulated at constant interfacial areas and constant box size in the normal direction.

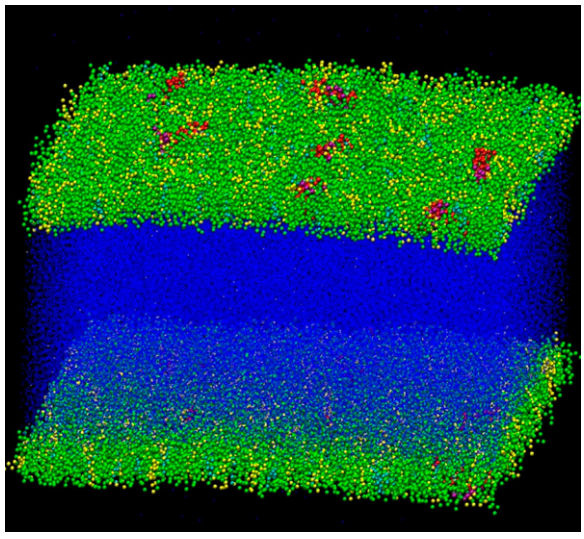

FIGURE 1 The simulation setup includes two lung surfactant model monolayers and a water slab. DPPC is shown in green, POPG in yellow, cholesterol in cyan, SP-C in red, water in blue, and Na^+ ions in gray.

CG force field parameters

We used an updated version of the CG force field by Marrink et al., (23), which also includes cholesterol. Compared with a previously published version (19), the new version of the CG force field includes more interaction energy levels without changing the form of the interaction potentials. It also has an increased number of particle subtypes compared with the earlier model to represent more accurately the chemical nature of the molecular fragments. For POPG lipids, the head group consists of two hydrophilic particles: the charged phosphate group is represented by a charged particle (Qa), the glycerol group is represented by a polar particle (P4). DPPC and cholesterol are standard components of the force field (23). For the protein, a CG force field was developed following the same strategy as that used by Marrink for lipids and detergents (19). As in the lipid force field, an approximate 4:1 mapping of heavy atoms to CG beads was used, with the exception of the aromatic side chains. A mapping of 2:1 or 3:1 was used for all cyclic structures to preserve their geometry. A reduced mass of 45 was used for all the cyclic-type particles. The N0 particle type was used for the backbone of each amino acid. Between zero and four beads were used to represent the amino acid side chains. The choice of the particle type for the amino acid side chains was based on the free energy of partitioning between water and hydrocarbons. Details of the parameterization and the full force field will be the subject of a separate publication (L. Monticelli, S. K. Kandasamy, X. Periole, R. G. Larson, D. P. Tieleman, S. J. Marrink, unpublished data).

For nonbonded interactions, the standard cutoffs for the CG force field were used: the Lennard-Jones interactions were shifted to zero between 0.9 and 1.2 nm, whereas the Coulomb potential was shifted to zero between 0 nm and 1.2 nm. The relative dielectric constant was 15, which is slightly lower than the value of 20 in the previous version of the force field.

Simulation details

Each monolayer contained 1280 DPPC lipids, 320 POPG lipids, 160 cholesterol molecules, and 14 SP-C proteins. All simulations used periodic boundaries in three dimensions. The water slab contained 126,282 water particles and 598 Na^+ ions. In the simulations at the constant volume of the box, no pressure coupling was used. The Berendsen barostat (coupling constant $\tau_P = 4.0$ ps) was used for the semi-isotropic pressure coupling in the compression/expansion runs. The system compressibility was set to 5×10^{-5} bar^{-1} in the lateral direction and to 0 in the normal direction. The latter ensures that the thickness of the vacuum slabs in the box changes as the area of the monolayer changes, without changing the size of the box normal to the membrane. Lipids and water with ions were coupled separately to the Berendsen heat bath (24) at $T = 310$ K with a coupling constant $\tau_T = 1$ ps. A time step of 20 fs was used. The neighborlist was updated every 10 steps.

Molecular dynamics simulations were performed using the GROMACS simulation package (25). A system with two monolayers in a liquid-expanded phase at the surface tension of 35 mN/m in the box of $35 \times 35 \times 50$ nm was used as a starting structure. Initial equilibration was performed for 5 ns at constant volume and temperature. The monolayer compression was simulated by applying positive lateral pressure to the system using the semi-isotropic pressure-coupling scheme (constant average pressure in the x-y plane and in the z-direction separately). Positive lateral pressure corresponds to negative surface tension imposed on each interface. The relation between the lateral pressure applied to the system, P_L, and the surface tension, γ_m, in each of the two (symmetric) monolayers reads as $\gamma_m = (P_N - P_L) \times L_z/2$, where L_z is the box size in the direction normal to the interfaces, P_N is the normal pressure, and $P_L = (P_{xx} + P_{yy})/2$. The presence

of the vacuum region bounding the water slab resulted in low values of the normal pressure (~0.3 bar). Negative surface tension at each interface destabilizes the flat geometry of the monolayer, inducing monolayer collapse. The compressed monolayers were expanded by applying negative lateral pressure to the system, using the semi-isotropic pressure coupling. Negative lateral pressure corresponds to positive surface tension imposed on each interface. The compression/expansion runs were performed for 50 ns using lateral pressures of 10, 2, −10, and −16 bar. An applied pressure of −16 bar corresponds to a surface tension of ~40 mN/m at each interface, similar to experimental values (3,26). An applied pressure of 10 bar corresponds to a negative surface tension of ~−25 mN/m imposed on each interface. This tension is not actually reached in the system (at a given lateral size of ~30 nm) because the monolayers collapse. Smaller monolayers (with lateral dimension of ~5 nm) exist in a metastable flat geometry under negative surface tension.

Production runs at constant volume and temperature (for 1 μs each) were performed on the systems previously compressed or expanded to interfacial areas of 1414, 1225, 1056, 876, and 645 nm^2, corresponding to surface tensions γ_m of 40, 35, 23, 0, and 23 mN/m (the last value refers to the monolayers after collapse). The systems contained either 1), two monolayers only; 2), two monolayers with a bilayer patch in the water subphase; or 3), two monolayers with an inverted bilayer patch in the vacuum subphase.

Each bilayer patch was 12 nm in diameter and contained 360 DPPC lipids, 90 POPG lipids, and 45 cholesterol molecules and 2 SP-C proteins. The bilayer patch (similar to a bicelle) was formed by equilibrating a square bilayer in a box of water larger than the bilayer (20 × 20 × 20 nm) for 10 ns with isotropic pressure coupling (1 bar). The box contained 64,911 water particles and 84 Na^+ ions. During the equilibration, the bilayer became circular, and the lipids bent at the perimeter to minimize the hydrocarbon chain-water contact area. The inverted bilayer patch (with hydrocarbon chains oriented outward) was formed by exchanging the position of the two leaflets of the circular bilayer patch. The inverted patch was equilibrated in vacuum (20 × 20 × 20 nm box) for 1 ns at constant volume and temperature.

RESULTS

Stability of lipid aggregates in the air and in the water subphases

We first investigated whether the monolayer-associated lipid reservoirs can be formed in the air and/or water subphases. To this end we simulated small preformed bilayer aggregates in the water and in the vacuum subphases adjacent to a monolayer and followed the change in the structure of these complexes.

In the first system, an inverted bilayer patch was placed in the vacuum subphase close to one of the monolayers in the simulation box (Fig. 2, 0 ns). We performed three simulations at different surface tensions in the monolayers (γ_m= 35, 23, 0 mN/m) at the constant volume for 1 μs each. The patch was unstable and readily fused with the adjacent monolayer (Fig. 2, 0.5 ns). Fusion was always observed irrespective of the degree of monolayer compression/expansion. The excess lipids were expelled into the water subphase during the fusion (Fig. 2, 5 ns) and remained connected to the monolayer at the interface. No evolution of the structure was observed on the simulation time scale.

In the second system, a lipid bilayer patch was placed in the water subphase close to one of the monolayers (Fig. 3, 0 ns). We performed four simulations at different surface tensions in the monolayers (γ_m= 40, 35, 23, 0 mN/m) at the constant volume of the box for 1 μs each. In most cases, the patch was stable in the water subphase (Fig. 3, 50 ns). Only in the case of a highly expanded monolayer (at γ_m= 40 mN/m) with large pores (Fig. 4, 0 ns) was the bilayer patch adsorbed on the interface in the pore region (Fig. 4, 5 ns). This process was, however, distinct from the fusion of a bilayer patch with a monolayer because the patch adsorbed directly at the bare water-vacuum interface. The lipids from the patch filled the pore region; however, the adsorption was not complete, and the residual bilayer aggregate with proteins remained on the interface (Fig. 4, 100 ns). On compression of the monolayer with the adsorbed bilayer patch (lateral pressure 2 bar, 50-ns simulation), the excess material was expelled into the water subphase and formed a circular bilayer aggregate. This bilayer aggregate did not detach from the monolayer in a subsequent simulation

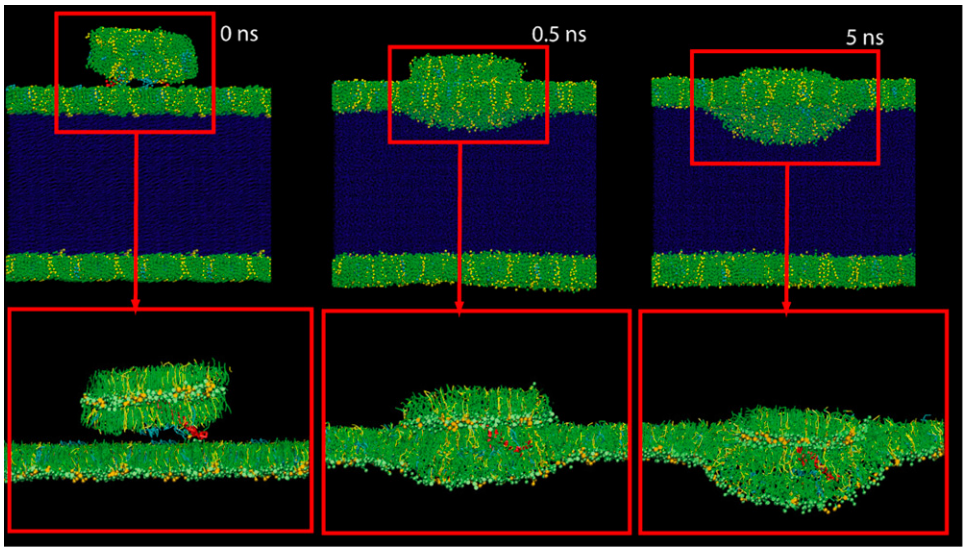

FIGURE 2 Two lung surfactant monolayers with an inverted circular bilayer patch in the vacuum subphase at 0, 0.5, and 5 ns. The inverted bilayer patch is unstable and readily fuses with the adjacent monolayer. Colors are as in Fig. 1.

(constant volume, 1 μs) and remained connected via a highly curved lipid region.

Monolayer-bilayer and bilayer-monolayer transformations

Next, we investigated the transformations between the monolayer and bilayer reservoirs during compression and expansion of the monolayer. The compression of the system with two monolayers ($\gamma_m = 35$ mN/m) was simulated by applying a positive lateral pressure to the system, which corresponds to imposing to a negative surface tension on each interface (see Methods). In two 50-ns simulations of monolayer compression, two different lateral pressures were applied (2 bar and 10 bar). Fig. 5 shows the evolution of the actual surface tension in the monolayer at an imposed surface tension on the interface of -25 mN/m (corresponding to a lateral pressure of 10 bar). On compression, the tension in the monolayer decreases gradually from the starting value (35 mN/m) to a slightly negative value but does not reach the applied value. When an expanded surfactant monolayer (Fig. 6, 0 ns, *top* and *side view*) is compressed, its surface becomes rippled (Fig. 6, 2 ns) when the surface tension approaches zero. If the applied lateral pressure is small (2 bar), the monolayer does not collapse. For larger values of the applied lateral pressure (10 bar), the monolayer begins to buckle as the tension in the monolayer becomes negative (Fig. 6, 5 ns). Buckling is characterized by out-of-plane deviations of the monolayer (corresponding to one bending wave per simulation box), which grow in amplitude with time (Fig. 6, 10 ns). Once the buckles form, the monolayer will collapse even if the compression is stopped. The monolayer collapses by folding into the water subphase (Fig. 6, 15 ns); collapse into the air subphase was never observed. After the monolayer buckling/collapse occurred, the system was simulated at constant volume for 1 μs.

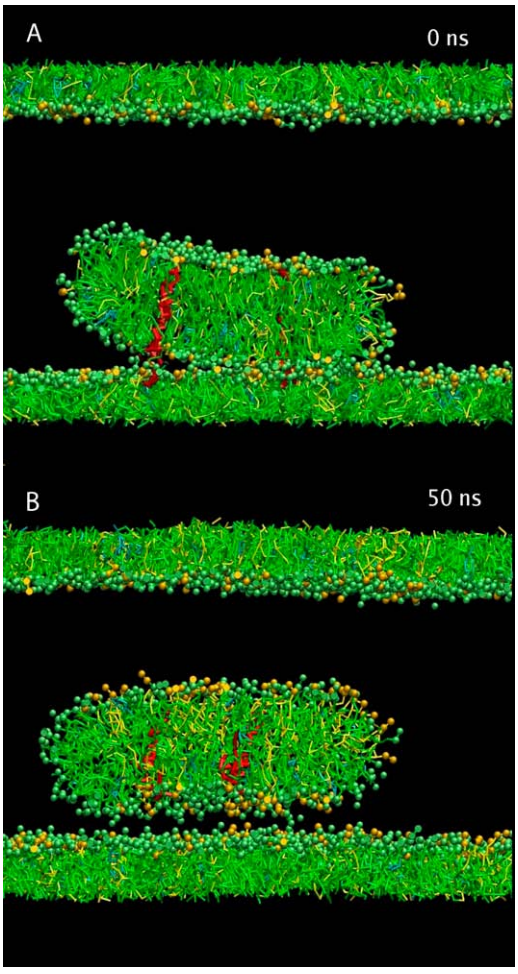

FIGURE 3 Two lung surfactant monolayers with a circular bilayer patch in the water subphase (water not shown) at (*A*) 0 ns and (*B*) 50 ns. Colors are as in Fig. 1.

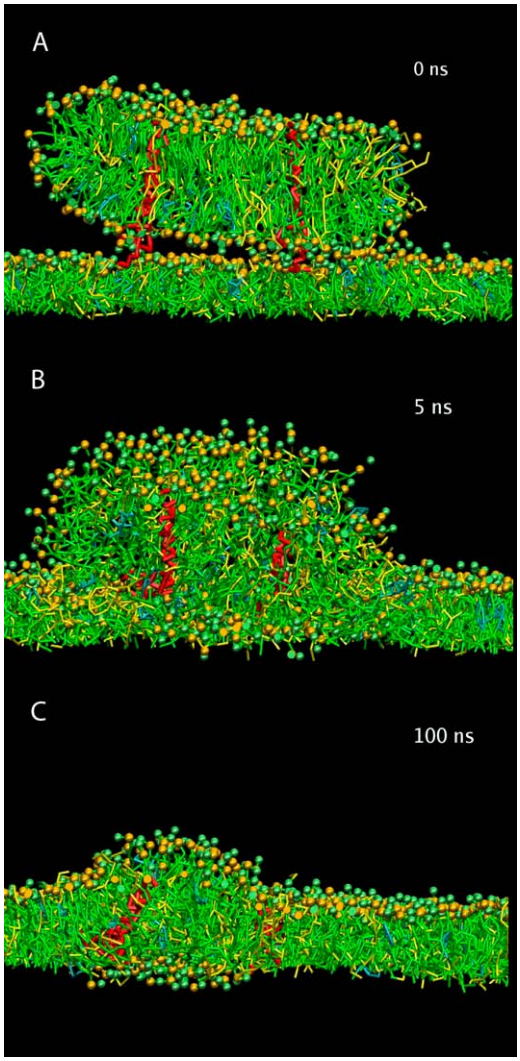

FIGURE 4 Adsorption of a bilayer patch in the pore region of an expanded monolayer (water not shown) at (*A*) 0 ns, (*B*) 5 ns, and (*C*) 100 ns. Colors are as in Fig. 1.

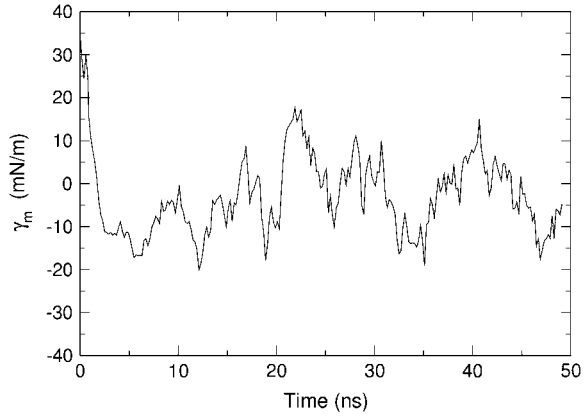

FIGURE 5 Surface tension in the monolayer compressed by a lateral pressure of 10 bar as a function of simulation time.

He bilayer folds in the water subphase are flat and are oriented approximately perpendicular to the monolayer. The folds either have a circular shape or are rectangular and periodic, spanning the simulation box (Fig. 7). They are connected to the monolayer through lipid regions of high negative curvature. The bilayer folds have the same lipid composition as the monolayer, and no segregation of SP-C or lipids is observed on the simulation time scale. The folds are stable during the simulation time; they do not change the shape and remain connected to the monolayer. The surfactant monolayer coexists with the bilayer folds at a surface tension of 23 mN/m, which is the equilibrium spreading tension for the studied system.

Using the compressed monolayers with folds as starting structures, we simulated expansion and further compression of the system. When the monolayer was compressed further, more material was expelled from the monolayer into the bilayer folds. Monolayer expansion was achieved by applying a negative lateral pressure to the system (−10 and −16 bar; 50 ns in both cases). On lateral expansion of the monolayer, the bilayer folds respread at the interface. Complete respreading of the material from the reservoirs at the interface occurs on the simulation time scale only if the imposed surface tension is larger than the monolayer equilibrium spreading tension.

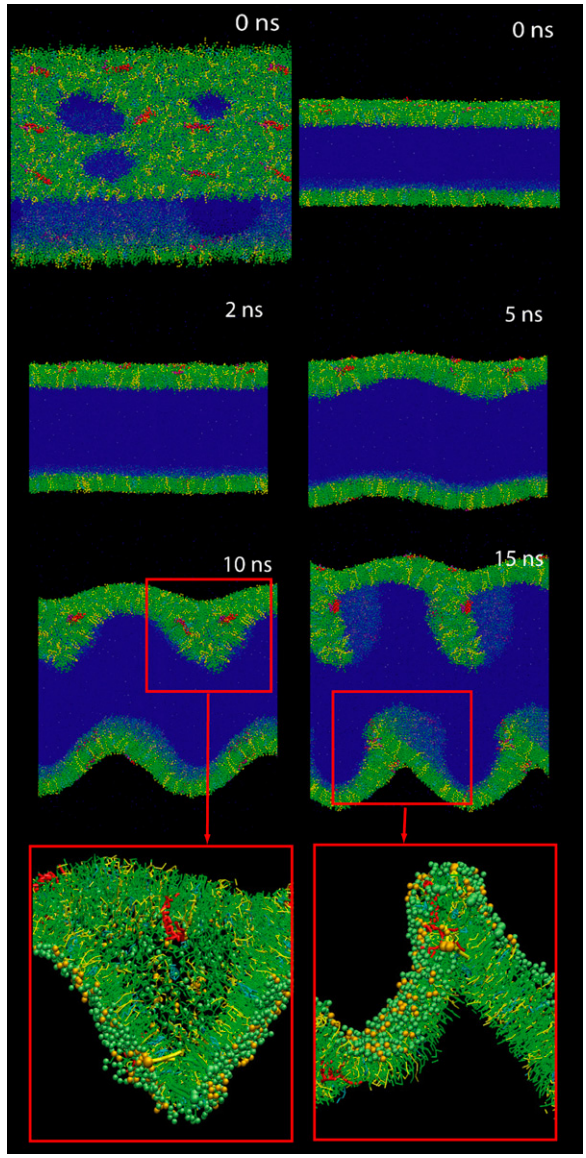

FIGURE 6 Collapse of the lung surfactant monolayer and formation of bilayer folds in the water subphase. On compression, an expanded monolayer with pores (0 ns, *top* and *side views*) forms a liquid-condensed phase (2 ns); the surface of the monolayer buckles (5 ns); the buckles grow in amplitude (10 ns); and the monolayer folds to form a bilayer (15 ns). DPPC is shown in green, POPG in yellow, cholesterol in cyan, SP-C in red, water in blue, and Na^+ ions in gray. Lipid head groups are represented as spheres, and lipid chains, cholesterol, and SP-C as sticks; the size of several selected lipid molecules is increased to show their conformation.

DISCUSSION

Lipid reservoirs connected to surfactant monolayer are essential for lung surfactant function (3–6). AFM experiments confirm that these reservoirs are lipid lamellar stacks containing one or several bilayers (4,13,27). However, in the AFM experiments lung surfactant is deposited on a substrate, and lipid aggregates are flattened; thus, information about the actual geometry and orientation of lipid reservoirs is lost by the deposition on the substrate. Hence, it is difficult to define the detailed structure of the lipid aggregates adopted on the alveolar gas exchange interface. It is also not clear whether these reservoirs are formed in the water or in the air subphase and what the molecular mechanism of their formation is.

The formation of lipid reservoirs connected to the lung surfactant monolayer is associated with reversible monolayer collapse by monolayer buckling and folding (13,28). The mechanism of monolayer collapse depends on the monolayer composition, which in turn determines molecular solubility and monolayer structure, morphology, and elastic properties

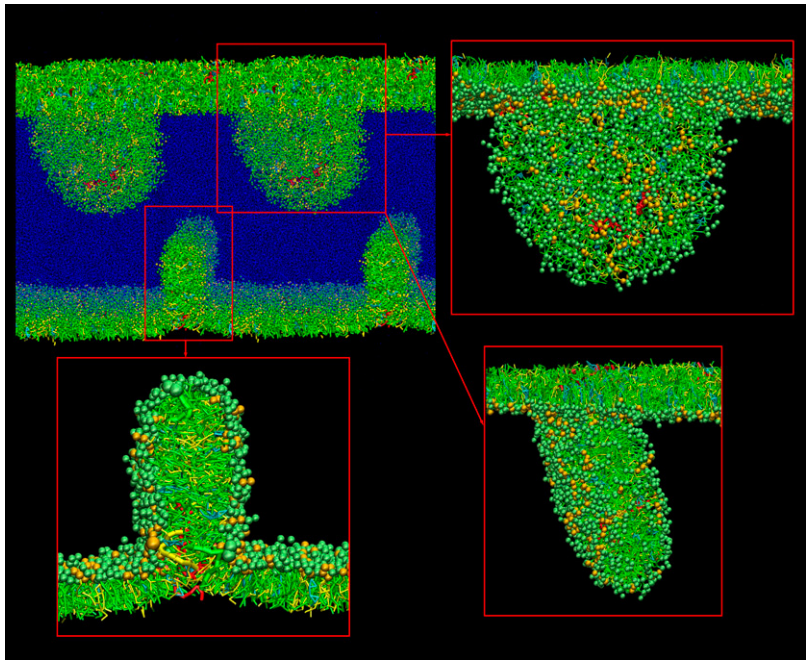

FIGURE 7 Bilayer folds (*circular on top* and *rectangular at the bottom*) attached to lung surfactant monolayers. Molecular representations are as in Fig. 6.

(13). It also depends on the compression rate (29). Monolayer collapse by folding into the water subphase has been observed experimentally for single-component and binary lipid mixtures (13,28), where the folds were identical in composition to the monolayer, as well as for lipid mixtures containing surfactant proteins SP-B and SP-C (11,30,31), where the proteins segregated in the folds. Earlier simulations of a monolayer collapse were carried out for the arachidic acid at the air-water interface using an atomistic model (32). In these simulations the molecules were ejected either into the air subphase or into the water subphase, forming small monolayer aggregates. However, this study was limited to a small box size (~6 nm), which did not allow monolayer bending and buckling to develop. Monolayer collapse has also been simulated for the long-chain PC lipids using a CG model (33), where a lipid bridge was formed in the air subphase. These simulations were also limited to a small system size (250 lipids in the monolayer) and a short simulation time (350 ps).

In this study we have simulated the collapse of a model lung surfactant monolayer on much larger length and time scales than previous studies. Collapse proceeds through buckling and folding into the water subphase and results in bilayer folds in the water subphase, never in the air subphase. The molecular composition of these folds is the same as in the monolayers, even though our simulations are long enough to allow significant lipid diffusion. When a bilayer fold is formed from a buckled monolayer in the water subphase, the contact area of the lipid chains with the air is reduced by approximately twice the area of the fold. This leads to a decrease of the surface energy of the lipid chain-air interface and thus to a decrease of the free energy of the system. The surface energy of the lipid chain-air interface can be estimated as the area times the surface tension at the hydrocarbon chain-air interface (29).

In the alternative scenario, lipid aggregates would form in the air subphase. The simulations clearly indicate that preformed lipid aggregates are unstable in the air subphase. In this case, the hydrocarbon chains of the excess lipids continue to be exposed to the air, and thus the surface energy would not decrease. The simulation results show that lipid reservoirs form in the water subphase, and we suggest that lipid reservoirs associated with a lung surfactant monolayer are likewise formed only in the water subphase.

Our simulations also provide a detailed molecular view of the structures of the monolayer-bilayer complexes and the transformation pathway. The simulations show that the bilayer folds remain connected to the lung surfactant monolayer, which coexists with folds at the equilibrium spreading tension of 23 mN/m. This behavior is consistent with experimental results on lung surfactant, where a plateau region is observed at ~22–25 mN/m in the tension-area isotherm, indicative of the monolayer coexistence with reservoirs. The simulations show that the folding of the monolayer is initiated by monolayer buckling. The monolayer buckling implies bending of a flat monolayer and thus requires overcoming an energy barrier. This energy barrier decreases with the decrease of the monolayer tension but remains finite until the monolayer tension becomes negative. In the simulations, this energy barrier also increases with the decrease of the monolayer lateral size (because the bending deformation is limited to one wavelength per simulation box because of the imposed three-dimensional periodicity). For the considered system size, the monolayer buckling and collapse were observed

on the simulation time scale only for negative monolayer tensions. The monolayer compression rates obtained in the simulations (~0.05–0.0005 Å^2/ns·molecule) are much faster than the experimental compression rates. They are also much faster than the monolayer relaxation rates, which drives the system substantially out of equilibrium. This can affect the value of the collapse tension (34) and also the mechanism of monolayer collapse (29).

The simulations also show that on repeated compression and expansion of the monolayer, there is a reversible exchange of material between the monolayer and the associated bilayer reservoirs. If the connectivity of the monolayer with the material in the bulk is lost, then the transfer of the material from the bulk to the interface is possible in two ways: either via fusion of the bulk lipid structures with the monolayer or via adsorption of the lipid structures on the bare air-water interface of pores in the highly expanded monolayer. To obtain the highly expanded monolayer with pores, the surface tension has to increase to nonphysiological levels above 35 mN/m. Thus, the lipid adsorption on the bare air-water interface of the pores in an expanded monolayer is probably not relevant for the functional lung. On the other hand, the process of fusion usually involves a high activation barrier (35), which would slow down the transfer of material from the bulk structures to the monolayer. Ineffective transfer of material to the interface would lead to an increase in the surface tension on monolayer reexpansion and may cause the loss of function. Based on these considerations, we propose that the connectivity of the bilayer aggregates in the water subphase to the monolayers is necessary for the reversibility of the monolayer-bilayer transformation. The latter maintains the low value of the surface tension in the monolayer at the air-water interface, which is essential for the function of lung surfactant.

In conclusion, we have simulated the reversible monolayer-bilayer transformations of a lung surfactant model system. Bilayer folds are formed in the water subphase on monolayer compression and respread from the bulk at the interface on monolayer expansion. The bilayer folds are stable lipid reservoirs that remain connected to the monolayer. The simulations indicate that the connectivity of lipid reservoirs to the monolayer is required for the reversibility of the exchange of material at low surface tensions.

S.B. is an Alberta Ingenuity postdoctoral fellow, L.M. is an Alberta Heritage Foundation for Medical Research (AHFMR) postdoctoral fellow, and D.P.T. is an AHFMR Senior Scholar and Canadian Institutes of Health Research New Investigator. This work was supported by the Natural Science and Engineering Research Council (Canada). Calculations were performed in part on WestGrid facilities.

REFERENCES

1. Wustneck, R., J. Perez-Gil, N. Wustneck, A. Cruz, V. B. Fainerman, and U. Pison. 2005. Interfacial properties of pulmonary surfactant layers. *Adv. Colloid Interface Sci.* 117:33–58.
2. Bachofen, H., and S. Schurch. 2001. Alveolar surface forces and lung architecture. *Comp. Biochem. Physiol. A.* 129:183–193.
3. Gunasekara, L., S. Schurch, W. M. Schoel, K. Nag, Z. Leonenko, M. Haufs, and M. Amrein. 2005. Pulmonary surfactant function is abolished by an elevated proportion of cholesterol. *Biochim. Biophys. Acta Mol. Cell. Biol.* 1737:27–35.
4. Leonenko, Z., S. Gils, S. Baoukina, L. Monticelli, J. Doehner, L. Gunasekara, F. Felderer, M. Rodenstein, L. M. Eng, and M. W. Amrein. 2007. An elevated level of cholesterol impairs self assembly of pulmonary surfactant into a functional film. *Biophys. J.* 93:674–683.
5. Schurch, S., R. Qanbar, H. Bachofen, and F. Possmayer. 1995. The surface-associated surfactant reservoir in the alveolar lining. *Biol. Neonate.* 67 (Suppl. 1):61–76.
6. vonNahmen, A., M. Schenk, M. Sieber, and M. Amrein. 1997. The structure of a model pulmonary surfactant as revealed by scanning force microscopy. *Biophys. J.* 72:463–469.
7. Bangham, A. D., C. J. Morley, and M. C. Phillips. 1979. The physical properties of an effective lung surfactant. *Biochim. Biophys. Acta.* 573:552–556.
8. Clements, J. A. 1977. Functions of the alveolar lining. *Am. Rev. Respir. Dis.* 115:67–71.
9. Watkins, J. C. 1968. The surface properties of pure phospholipids in relation to those of lung extracts. *Biochim. Biophys. Acta.* 152:293–306.
10. Piknova, B., W. R. Schief, V. Vogel, B. M. Discher, and S. B. Hall. 2001. Discrepancy between phase behavior of lung surfactant phospholipids and the classical model of surfactant function. *Biophys. J.* 81:2172–2180.
11. Takamoto, D. Y., M. M. Lipp, A. von Nahmen, K. Y. C. Lee, A. J. Waring, and J. A. Zasadzinski. 2001. Interaction of lung surfactant proteins with anionic phospholipids. *Biophys. J.* 81:153–169.
12. Yu, S. H., and F. Possmayer. 2003. Lipid compositional analysis of pulmonary surfactant monolayers and monolayer-associated reservoirs. *J. Lipid Res.* 44:621–629.
13. Lipp, M. M., K. Y. C. Lee, D. Y. Takamoto, J. A. Zasadzinski, and A. J. Waring. 1998. Coexistence of buckled and flat monolayers. *Phys. Rev. Lett.* 81:1650–1653.
14. Lewis, J. F., and R. Veldhuizen. 2003. The role of exogenous surfactant in the treatment of acute lung injury. *Annu. Rev. Physiol.* 65:613–642.
15. Panda, A. K., K. Nag, R. R. Harbottle, K. Rodriguez-Capote, R. A. Veldhuizen, N. O. Petersen, and F. Possmayer. 2004. Effect of acute lung injury on structure and function of pulmonary surfactant films. *Am. J. Respir. Cell. Mol.* 30:641–650.
16. Kandasamy, S. K., and R. G. Larson. 2005. Molecular dynamics study of the lung surfactant peptide SP-B1–25 with DPPC monolayers: Insights into interactions and peptide position and orientation. *Biophys. J.* 88:1577–1592.
17. Kaznessis, Y. N., S. Kim, and R. G. Larson. 2002. Specific mode of interaction between components of model pulmonary surfactants using computer simulations. *J. Mol. Biol.* 322:569–582.
18. Lee, H., S. K. Kandasamy, and R. G. Larson. 2005. Molecular dynamics simulations of the anchoring and tilting of the lung-surfactant peptide SP-B1–25 in palmitic acid monolayers. *Biophys. J.* 89:3807–3821.
19. Marrink, S. J., A. H. de Vries, and A. E. Mark. 2004. Coarse grained model for semiquantitative lipid simulations. *J. Phys. Chem. B.* 108:750–760.
20. Marrink, S. J., and A. E. Mark. 2004. Molecular view of hexagonal phase formation in phospholipid membranes. *Biophys. J.* 87:3894–3900.
21. Marrink, S. J., J. Risselada, and A. E. Mark. 2005. Simulation of gel phase formation and melting in lipid bilayers using a coarse grained model. *Chem. Phys. Lipids.* 135:223–244.
22. Rodriguez-Capote, K., K. Nag, S. Schurch, and F. Possmayer. 2001. Surfactant protein interactions with neutral and acidic phospholipid films. *Am. J. Physiol. Lung Cell. Mol. Physiol.* 281:L231–L242.
23. Marrink, S. J., H. J. Risselada, S. Yefimov, D. P. Tieleman, and A. H. de Vries. 2007. The MARTINI forcefield: coarse grained model for biomolecular simulations. *J. Phys. Chem. B.* 111:7812–7824.

24. Berendsen, H. J. C., J. P. M. Postma, W. F. van Gunsteren, A. DiNola, and J. R. Haak. 1984. Molecular dynamics with coupling to an external bath. *J. Chem. Phys.* 81:3684–3690.

25. Lindahl, E., B. Hess, and D. van der Spoel. 2001. GROMACS 3.0: a package for molecular simulation and trajectory analysis. *J. Mol. Model.* 7:306–317.

26. Wu, C. W., S. L. Seurynck, K. Y. C. Lee, and A. E. Barron. 2003. Helical peptoid mimics of lung surfactant protein C. *Chem. Biol.* 10:1057–1063.

27. Malcharek, S., A. Hinz, L. Hilterhaus, and H. J. Galla. 2005. Multilayer structures in lipid monolayer films containing surfactant protein C: effects of cholesterol and POPE. *Biophys. J.* 88:2638–2649.

28. Gopal, A., and K. Y. C. Lee. 2001. Morphology and collapse transitions in binary phospholipid monolayers. *J. Phys. Chem. B.* 105:10348–10354.

29. Ybert, C., W. X. Lu, G. Moller, and C. M. Knobler. 2002. Collapse of a monolayer by three mechanisms. *J. Phys. Chem. B.* 106:2004–2008.

30. Kramer, A., A. Wintergalen, M. Sieber, H. J. Galla, M. Amrein, and R. Guckenberger. 2000. Distribution of the surfactant-associated protein C within a lung surfactant model film investigated by near-field optical microscopy. *Biophys. J.* 78:458–465.

31. Seifert, M., D. Breitenstein, U. Klenz, M. C. Meyer, and H. J. Galla. 2007. Solubility vs. electrostatics: What determines the lipid/protein interaction in the lung surfactant. *Biophys. J.* 93:1192–1203.

32. Lorenz, C. D., and A. Travesset. 2006. Atomistic simulations of Langmuir monolayer collapse. *Langmuir.* 22:10016–10024.

33. Nielsen, S. O., C. F. Lopez, P. B. Moore, J. C. Shelley, and M. L. Klein. 2003. Molecular dynamics investigations of lipid Langmuir monolayers using a coarse-grain model. *J. Phys. Chem. B.* 107:13911–13917.

34. Rugonyi, S., E. C. Smith, and S. B. Hall. 2004. Transformation diagrams for the collapse of a phospholipid monolayer. *Langmuir.* 20:10100–10106.

35. Kozlovsky, Y., and M. M. Kozlov. 2002. Stalk model of membrane fusion: solution of energy crisis. *Biophys. J.* 82:882–895.

36. Baoukina, S., L. Monticelli, S. J. Marrink, and D. P. Tieleman. *Langmuir.* In press.